Interface sharpening and broadening during annealing of Cu/Ni multilayers: A kinetic Monte Carlo study

Jean-Marc Roussel
Laboratoire TECSEN, UMR 6122 CNRS, Université Paul Cézanne, Aix-Marseille III, Faculté des Sciences et Techniques de Saint-Jérôme, Case 262, 13397 Marseille Cedex 20, France

Pascal Bellon
Department of Materials Science and Engineering, University of Illinois at Urbana-Champaign, Urbana, Illinois 61801, USA
(Received 13 September 2005; published 2 February 2006)

Kinetic Monte Carlo simulations are performed to study the evolution of interfaces in a model alloy system whose parameters are chosen so as to reproduce the main features of the Cu-Ni system, in particular the asymmetry of diffusion coefficients. Recently, Erdélyi *et al.* [Phys. Rev. Lett. **89**, 165901 (2002)] have shown that, in alloy systems forming ideal solid solutions, a large asymmetry can lead to the unexpected transient sharpening of interfaces that were initially flat and diffuse. In the present work we first remove two simplifications made by these authors and we study the consequences on the sharpening and broadening of interfaces during the annealing of a multilayered sample. First, in our diffusion model, atoms migrate by vacancy-assisted jumps instead of direct atom exchanges. Second, we investigate the effect of the initial roughness of interfaces on their evolution during annealing. In addition, we also study the influence of the short-range order that arises from a nonideal solid solution, since the Cu-Ni phase diagram displays a miscibility gap at low temperatures. While we observe that the transient sharpening phenomenon can still take place with a vacancy mechanism in alloys with large diffusional asymmetries, we find that the sharpening amplitude is reduced when short-range order is present and even suppressed when interfaces are initially rough. In the latter case, the in-plane wavelength of the roughness plays a determinant role and we identify a crossover from sharpening to broadening when this wavelength exceeds a threshold value. The practical implications of these effects are discussed.

DOI: 10.1103/PhysRevB.73.085403 PACS number(s): 68.35.Fx, 68.35.Ct, 64.75.+g, 68.35.Dv

I. INTRODUCTION

While atomic diffusion in solid-state alloys is a relatively mature field, microstructural evolutions in concentrated alloys may nevertheless be nontrivial since they involve a very large number of atomic jump frequencies, which often depend quite sensitively on the chemical nature of the migrating atom and of its local atomic environment. In particular, in an *A*-*B* binary alloy system, diffusion coefficients are often asymmetric in the sense that one species diffuses faster than the other, as demonstrated by Kirkendall and coworkers in their seminal experiment.[1] Moreover, the atomic jump frequencies for one species may significantly vary with the local composition, leading to composition dependent diffusion coefficients. Erdélyi and co-workers[2–4] have recently shown that this composition dependence can lead to unexpected and counterintuitive evolutions. They showed, using deterministic kinetic modeling and kinetic Monte Carlo (KMC) simulations, that in an ideal *A*-*B* system, this composition dependence can lead to a transient sharpening of *A*/*B* planar interfaces that were initially diffuse. This is particularly remarkable since at long times the system has to reach a homogeneous state, as dictated by thermodynamics forces, which are reduced here to configurational entropy. Such a transient interface sharpening in a miscible alloy has been evidenced experimentally in Mo/V multilayers by x-ray diffraction,[5] where a short annealing at 953 K reduced the interfacial thicknesses from about 1.5 nm initially to 0.8 nm. The same authors proposed that this effect could be of practical interest since sharp interfaces are highly desirable in many layered structures, including multilayers for x-ray mirrors and for quantum electronic devices.

In the models used by Erdélyi and co-workers,[2–4] diffusion proceeds by direct exchange of atoms, and it is thus characterized by one diffusion coefficient D. In an $A_{1-c}B_c$ homogeneous alloy, these authors assume that the composition dependence of this diffusion coefficient follows $D(c)=D(0)\exp(mc)$, where the parameter m characterizes the degree of the asymmetry of the diffusion coefficient. At the atomic scale, using a broken bond model,[3,6] this asymmetry can also be expressed in terms of the difference between the strength of the *A*-*A* and *B*-*B* pairwise interaction energies, $m=-Z(\epsilon_{AA}-\epsilon_{BB})/kT$, where Z is the coordination number for the first nearest-neighbor shell. According to the simulation results obtained by Erdélyi and co-workers for binary alloy systems with large asymmetry, choosing for instance diffusion to decrease as the local *B* concentration increases, i.e., $m<0$, the sharpening effect is due to the fact that the tail of the initial *B* composition profile, having a local composition that is almost pure *A*, dissolves rapidly in this *A*-rich phase before any intermixing can take place near the center of the composition profile. This rapid dissolution of the tail of the *B* composition profile leads to a shift of the interface position and to an increase of the composition gradient, i.e., to interface sharpening. However, this tail dissolution, which proceeds through a layer-by-layer mode, progressively increases

the B concentration in the A-rich region, and thus reduces the effect of the diffusion asymmetry. Eventually, the sharpening reaches a maximum and interfaces begin to broaden, leading to the complete mixing of the A-rich and B-rich regions.

The conclusions reached by Erdélyi and co-workers, however, are potentially affected by the simplifications made in the models used for the simulations, and in the physical situations they considered. In this work, we focus on the Cu-Ni alloy, for which specific information on atomic jump frequencies is available, and we relax three important constraints used by Erdélyi and co-workers. First, we consider here models where atomic diffusion proceeds by vacancy jumps, since this is the correct mechanism for nearly all practical situations, and in particular for Cu-Ni. As a result, one needs now to define two diffusion coefficients, and thus two asymmetry parameters, a first one related to the composition dependence of the vacancy formation energy, and a second one related to the composition dependence of the vacancy migration energy. For a given alloy system, these asymmetries can be assessed by calculating the difference in formation and migration energies of the vacancy in the pure phases, ΔE^f and ΔE^m, respectively. At the vicinity of an interface the composition varies strongly over short distances, and thus vacancy diffusion paths can be significantly affected by these two asymmetries, leading to microstructural evolutions that may differ from those obtained with a direct atom-exchange mechanism. For instance, in previous studies on the coarsening of precipitates in a binary alloy during thermal annealing,[7,8] KMC simulations revealed that the above asymmetries can change the main coarsening mechanism from evaporation-condensation to coagulation during the early stages of the coarsening, and that would change the time evolution of the composition of the precipitates. Recent experiments on Al-Ag and Al-Zn systems, studied by coherent x-ray scattering, through analysis of the fluctuations of speckle intensity, support the idea that diffusion asymmetry can change the dominant coarsening mechanism.[9] We note that in the simplified diffusion model used for the above simulation studies,[7,8] ΔE^f and ΔE^m were related to one another, and thus that this model had only one independent asymmetry parameter. In this study, we will develop an extension of this diffusion model such that ΔE^f and ΔE^m are independent.

In the context of the present work, it is important to note that in most metallic binary alloys, the values of both ΔE^m and ΔE^f terms are not small compared to the vacancy formation and migration energies. We choose the Cu-Ni system to illustrate the effects of vacancy mechanism and of diffusion asymmetry on interfacial evolutions. For that system, recent compilation of experimental data for pure Cu and pure Ni gives $E^f_{Cu}=1.28\pm0.05$ eV, $E^f_{Ni}=1.79\pm0.05$ eV, $E^m_{Cu}\approx0.70\pm0.02$ eV, and $E^m_{Ni}=1.04\pm0.04$ eV and thus $\Delta E^f=-0.5\pm0.1$ eV and $\Delta E^m=-0.34\pm0.06$ eV.[10] This corresponds to a marked asymmetry of the atomic mobilities, i.e., a Ni solute atom diffuses much faster in Cu than a solute Cu does in Ni, and the Ni diffusion in a Cu-rich region increases significantly as the Cu concentration of that region increases. In addition, Cu and Ni crystals both form face-centered-cubic (fcc) lattices, and the two elements possess a small lattice mismatch, $\Delta a/a\approx0.025$, so that we have neglected stress effects on diffusion in the present study. Finally, this system is close to an ideal mixture, with a complete miscibility in the solid state at temperatures exceeding 628 K, which is the top of the miscibility gap.[11–13] A small modification of the model parameters will allow us to turn off the tendency for phase separation in our simulations, so as to study its impact on interfacial evolutions. We will show here that the short-range order (SRO) that results from the tendency for phase separation has a direct effect on interfacial evolution, a point that was not considered in the works published so far by Erdélyi *et al.*[4]

A third limitation in Erdélyi and co-workers studies is that interfaces are assumed to be planar (i.e., with no in-plane roughness). One advantage of that assumption is that there is no loss of information when the full three-dimensional composition field is projected onto the normal of a multilayered structure to obtain a one-dimensional composition profile. The drawback, however, is that the interfacial roughness is null and is assumed to remain so during annealing. This may be a significant limitation to the practical application of interface sharpening since most multilayers display some amount of roughness in their as-grown state. From a characterization standpoint, common techniques only provide a one-dimensional profile, and thus yield an apparent width of the interface. This apparent width or diffuseness, however, contains contributions from the true diffuseness as well as from the roughness of the interface. Advanced techniques make it possible to extract separately these two quantities.[14–17] This distinction is important since we will show here that rough interfaces can develop evolutions far different from those observed for flat (planar) interfaces. In particular, we find that, keeping constant the initial amplitude of the roughness, if one follows the evolution of the interface through a one-dimensional composition profile, the sharpening effect during annealing is suppressed as the wavelength of the roughness increases, and even disappears above a threshold wavelength.

The paper is organized as follows. In Sec. II A, we introduce the atomistic model used to calculate the vacancy jump frequencies; two sets of parameters are considered, the first one approximates the Cu-Ni system by an ideal solid solution, while the second includes the small and positive heat of mixing of that alloy system. In Sec. II B, we perform KMC simulations in equilibrium Cu-Ni solid solutions, in order to measure the composition dependence of the Cu and Ni diffusion coefficients. We then use KMC simulations to assess the evolution of Cu/Ni {111} interfaces that, initially, are sharp and flat in Sec. III A, diffuse and flat in Sec. III B, and sharp but sinusoidally rough in Sec. III C.

II. MODEL

A. Diffusion model with vacancy mechanism

Energetics. We consider a A-B binary alloy with a highly diluted vacancy (V) concentration on a rigid lattice with an fcc structure (the number of first neighbors $Z=12$). The energetics is based on an Ising-like model that depends on two terms:

$\epsilon = \epsilon_{AA} + \epsilon_{BB} - 2\epsilon_{AB}$, where ϵ_{ij} terms represent pair interactions between i and j atoms and, ϵ is an effective pair interaction between atoms. For fcc structures, it is small beyond first neighbors,[18] and we restrict ourselves to first nearest-neighbor interactions here. ϵ is directly related to the bulk phase diagram of the system considered. Its sign gives the tendency towards ordering ($\epsilon > 0$) or towards phase separation ($\epsilon < 0$). For the Cu-Ni system, we use $\epsilon = -0.022$ eV to obtain a critical temperature for phase separation of $T_c = 625$ K, at $c = 0.5$, in order to reproduce the experimental value $T_c^{\text{exp}} = 628$ K, for a Ni concentration of $c = 0.67$.[11–13]

$u = \epsilon_{AA} - \epsilon_{BB}$, which accounts for the difference in vacancy formation energies $\Delta E^f = -Zu/2$ in the two pure phases. The system being highly diluted with respect to vacancies, u does not affect the equilibrium phase diagram. Its sign gives the tendency of the vacancy to occupy A-rich regions ($u > 0$) or B-rich regions ($u < 0$). For A=Cu and B=Ni, we use $u = 0.0633$ eV, leading to a difference in vacancy formation energies $\Delta E^f = -0.38$ eV, a value close to the experimental one.

Kinetics. Diffusion occurs via vacancy (V) jumps toward nearest-neighbor X atoms, where X equals A or B. Atom-vacancy exchange frequencies are calculated using rate theory with a constant attempt frequency $\nu = 10^{14}$ s^{-1}. We first consider a model where the activation energy E^{VX} for these jumps is derived from the broken bond model previously described in Refs. 6, 7, and 22 and corresponds to the energy required to move an X atom from its initial stable site to the XV saddle point. Notice that in this model, hereafter referred to as model I, the contribution of the jumping atom to the saddle-point configuration energy is taken as a constant. E_{I}^{VX} writes

$$E_{\text{I}}^{\text{VA}} = E_2^{\text{A}} - n_{\text{A}}^{\text{A}} \frac{\epsilon + u}{2},$$

$$E_{\text{I}}^{\text{VB}} = E_2^{\text{B}} - n_{\text{B}}^{\text{B}} \frac{\epsilon - u}{2}, \tag{1}$$

where n_{A}^{X} and n_{B}^{X} are the number of A and B nearest neighbors of the atom X to be exchanged with the vacancy V. The term E_2^{X} is the activation energy for a vacancy exchange with a X solute atom. The vacancy migration energy E_0^{X} in a pure matrix depends directly on E_2^{X}, ϵ and u in this model. The difference in vacancy migration energy between the two pure elements writes $\Delta E^m = E_0^{\text{A}} - E_0^{\text{B}} = E_2^{\text{A}} - E_2^{\text{B}} + 2\Delta E^f (Z-1)/Z$. Because of this constraint between ΔE^m and ΔE^f, if one chooses values for E_2^{X} and ΔE^f that correspond to Cu-Ni, ΔE^m is overestimated by more than 50%, as seen in Fig. 1. Model I is therefore not well suited to reproduce simultaneously ΔE^f and ΔE^m for the Cu-Ni system. To address this deficiency, and better reproduce self- and solute diffusion data for the Cu-Ni system, one needs to make E_0^{X} and E_2^{X} independent. This can be achieved by using a modified model, hereafter denoted as model II, where the saddle-point energy now depends on the local chemical environment. Consider first the exchange of an A atom with a vacancy. In order to satisfy detailed balance, the simplest extension of model I that includes an environment dependence in the contribution of the migrating atom to the saddle-point energy takes the form

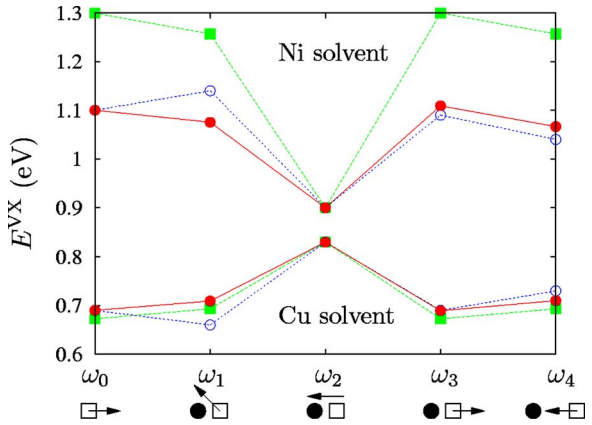

FIG. 1. (Color online) Activation energies from (■) model I [Eq. (1)], from (•) model II [Eq. (3) with $\epsilon = -0.022$ eV], and from (○) EAM calculations (Ref. 19) for the five ω's frequencies. In the usual notation (Refs. 20 and 21), ω_0 is the solvent atom-vacancy exchange frequency, ω_2 is the frequency of solute-vacancy exchanges, ω_1 is the frequency of atom-vacancy exchanges that do not dissociate the solute-vacancy pair, ω_3 is the frequency of an atom-vacancy exchange that dissociates the solute-vacancy pair, and ω_4 is the frequency of an atom-vacancy exchange that associates the solute and the vacancy.

$$E_{\text{II}}^{\text{VA}} = K_0 + K_1 (n_{\text{A}}^{\text{A}} + n_{\text{A}}^{\text{V}}) - n_{\text{A}}^{\text{A}} \frac{\epsilon + u}{2}, \tag{2}$$

where n_{A}^{V} is the number of A nearest neighbors of the vacancy, excluding the migrating A, and K_0 and K_1 are constants. The value of these constants are determined by imposing that the activation energies for solute and solvent diffusion are E_2^A and E_0^A, respectively.

The extension of the above procedure to the migration of B atoms is straightforward. Activation energies for XV exchanges in this model II can be expressed in the following compact form:

$$E_{\text{II}}^{\text{VA}} = E_{\text{I}}^{\text{VA}} + \frac{n_{\text{A}}^{\text{A}} + n_{\text{A}}^{\text{V}}}{2(\text{Z}-1)} \left(E_0^{\text{A}} - E_2^{\text{A}} + (\text{Z}-1) \frac{\epsilon + u}{2} \right),$$

$$E_{\text{II}}^{\text{VB}} = E_{\text{I}}^{\text{VB}} + \frac{n_{\text{B}}^{\text{B}} + n_{\text{B}}^{\text{V}}}{2(\text{Z}-1)} \left(E_0^{\text{B}} - E_2^{\text{B}} + (\text{Z}-1) \frac{\epsilon - u}{2} \right). \tag{3}$$

The parameters of this model II are fitted to two of the five activation energies for the vacancy-atom exchanges in infinitely dilute Cu-Ni alloys:[21] the parameters E_0^{X} and E_2^{X} are set to the values calculated by Adams *et al.*,[19] who used interatomic potentials based on the embedded atom method. The remaining three frequencies are given in Table I from model II and compared to the EAM energies. The agreement between model II and Adams' data is much better than that between model I and Adams' data.

Finally, we will consider in this work another set of parameters to study the role of the phase-separation tendency on kinetics. This second set of parameters describes a Cu-Ni-like system that does not present any miscibility gap.

TABLE I. Activation energies from model II [Eq. (3)] compared to the EAM activations energies from Ref. 19 for vacancy jumps near the impurity (see Fig. 1 for the ω's definition). To simplify the table, additional terms ΔE_α^X, ΔE_β^X have been defined as follows: $\Delta E_\alpha^A=[E_0^A-E_2^A+(Z-1)(\epsilon+u)/2]/(2Z-2)$, $\Delta E_\alpha^B=[E_0^B-E_2^B+(Z-1)\times(\epsilon-u)/2]/(2Z-2)$, $\Delta E_\beta^A=(E_0^A-E_2^A)(Z-2)/(Z-1)$, and $\Delta E_\beta^B=(E_0^B-E_2^B)(Z-2)/(Z-1)$. The differences in formation energies ΔE^f and in migration energies ΔE^m are also reported. A=Cu and B=Ni.

Cu solvent and Ni impurity				
Jump	E_{II}^{VX}	$CuNi^0$	$CuNi^\epsilon$	EAM (Ref. 19)
ω_0	E_0^A	0.69	0.69	0.69
ω_1	$E_2^A-\Delta E_\beta^A$	0.71	0.71	0.66
ω_2	E_2^B	0.83	0.83	0.83
ω_3	$E_0^A+\Delta E_\alpha^A$	0.68	0.69	0.69
ω_4	$E_0^A+(\epsilon+u)/2+\Delta E_\alpha^A$	0.71	0.71	0.73
ω_4/ω_3	$(\epsilon+u)/2$	0.03	0.02	0.04
Ni solvent and Cu impurity				
Jump	E_{II}^{VX}	$CuNi^0$	$CuNi^\epsilon$	EAM (Ref. 19)
ω_0	E_0^B	1.10	1.10	1.10
ω_1	$E_2^B-\Delta E_\beta^B$	1.08	1.08	1.14
ω_2	E_2^A	0.90	0.90	0.90
ω_3	$E_0^B+\Delta E_\alpha^B$	1.10	1.11	1.09
ω_4	$E_0^B+(\epsilon-u)/2+\Delta E_\alpha^B$	1.07	1.07	1.04
ω_4/ω_3	$(\epsilon-u)/2$	−0.03	−0.04	−0.05
ΔE^f	$-Zu/2$	−0.38	−0.38	−0.384
ΔE^m	$E_0^A-E_0^B$	−0.41	−0.41	−0.41

Practically, this is achieved by setting $\epsilon=0$, and keeping unchanged all other parameters, u, E_0^X, and E_2^X. In Table I, we report the values of the corresponding five jump frequencies with this second set of parameters. For the sake of clarity, we will hereafter denote as $CuNi^\epsilon$ the system with $\epsilon=-0.022$ eV, and $CuNi^0$ the one with $\epsilon=0$.

B. Diffusion asymmetry in Cu-Ni

In this section we measure diffusion coefficients in equilibrium $Cu_{1-c}Ni_c$ solid solutions, in particular in concentrated alloys, for the two sets of parameters for the diffusion model II introduced above. Starting first with dilute alloys, i.e., for $c\to 0$ and $c\to 1$, one can use the classical theory of atomic diffusion that provides us with analytical expressions for self-diffusion and solute diffusion coefficients.[20,21] Let us simply recall that the diffusion coefficient of an isolated solute atom B $(c\to 0)$ is calculated to be

$$D_{B^*}^A = a^2\omega_2 c_v \frac{\omega_4}{\omega_3} f_2, \tag{4}$$

where all ω's are defined in Fig. 1, c_v is the vacancy concentration in the A matrix, and f_2 is the correlation factor between successive solute-vacancy exchanges

$$f_2 = \frac{\omega_1 + \omega_3 3.5F(\omega_4/\omega_0)}{\omega_1 + \omega_2 + \omega_3 3.5F(\omega_4/\omega_0)}, \tag{5}$$

where F is a polynomial function of ω_4/ω_0.[21] Formula (4) gives also the thermal self-diffusion coefficient of an A tracer atom when setting all ω's equal to ω_0:

$$D_{A^*}^A = a^2\omega_0 c_v f_0, \tag{6}$$

where the geometric correlation factor $f_0=[1+3.5F(1)]/[2+3.5F(1)]=0.7815$ for fcc crystal.

It is worth noting that in order to assess the mobility asymmetry $\ln(D_{B^*}^A/D_{A^*}^B)$ between pure A and pure B regions of a A/B multilayer, one has to take into account the fact that, in Eq. (4), the vacancy concentration is a function of the local composition. Assuming that the vacancy concentration has reached its equilibrium value, the magnitude of this contribution to the atomic mobility asymmetry is given by $\exp(\Delta E^f/kT)$.

Turning now to concentrated alloys, we employ KMC simulations with a residence time algorithm to calculate diffusion coefficients for our diffusion model.[22,23] We use the activation energies from Eq. (3) and the two alloy systems introduced in Sec. II A, $CuNi^\epsilon$ and $CuNi^0$. To calculate the tracer diffusion coefficients, we label every A or B atom and first compute the time-dependent diffusion coefficient $D_{X^*}(t)=\langle\delta R^2(t)\rangle_{X^*}/6\delta t$, where δR denotes the displacement of the X atoms and $\langle\rangle_{X^*}$ stands for the average over the $X=A$ or B tagged atoms. The tracer diffusion coefficient D_{X^*} is recovered at large time. A face-centered-cubic crystal of size 512 sites with periodic boundary conditions is large enough to calculate the quantities of interest. The initial condition consists of a disordered alloy where the number of A and B is fixed by the concentration c considered. Only one vacancy is introduced in the crystal and the diffusion coefficients are therefore calculated at constant vacancy concentration $c_v=1.9\times10^{-3}$.

In Fig. 2(a), we report the diffusion coefficients D_{Ni^*} and D_{Cu^*} versus the Ni concentration c for two different temperatures $T=650$ K and $T=1000$ K. By first examining the dilute cases, it is important to note that $D_{Ni^*}^{Cu}$ is greater that $D_{Cu^*}^{Ni}$ by about one order of magnitude at $T=650$ K and by a factor ≈4 at $T=1000$ K. Additionally, the two parametrizations used for Cu-Ni give similar solute diffusion coefficients for the range of temperature considered. In concentrated alloys, the difference between $CuNi^\epsilon$ and $CuNi^0$ systems is very small at $T=1000$ K. The tracer diffusion coefficients atoms for both parametrizations follow relatively closely an exponential dependence with c at this high temperature. From Fig. 2(a), the diffusion coefficients can be written:

$$D_{X^*}(c) \approx D_{X^*}(0)[D_{X^*}(1)/D_{X^*}(0)]^c, \tag{7}$$

where X=Cu or Ni, and c refers to the Ni concentration. This behavior suggests that, at this high temperature, the vacancy migration energy is given by a linear combination of the migration energies for the pure elements, weighted by the concentrations. At lower temperature, however, the tracer diffusion coefficients for the $CuNi^\epsilon$ model deviate significantly from an exponential dependence, as seen on Fig. 2(a)

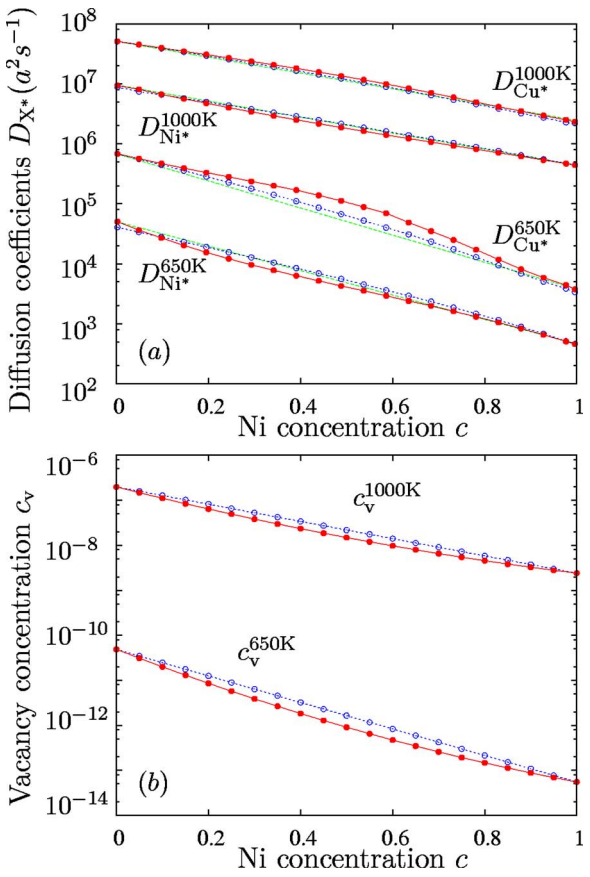

FIG. 2. (Color online) Composition dependence of the diffusion coefficients in a $Cu_{1-c}Ni_c$ solid solution at $T=650$ K and $T=1000$ K. (a) the coefficients for tracers Ni^* and Cu^* are calculated from KMC simulations using the activation model of Eq. (3) with (•) the $CuNi^{\epsilon}$ parameters and (◦) the $CuNi^0$ ones (see text in Sec. II A) at constant vacancy concentration $c_v=1.9\times10^{-3}$. The exponential dependences of Eq. (7) are represented by thin lines. (b) Composition dependence of the vacancy concentration c_v estimated from Eq. (8) for both $CuNi^{\epsilon}$ and $CuNi^0$ systems.

for $T=650$ K. Since the deviation is much smaller for the $CuNi^0$ system, and since it is suppressed as temperature increases, we conclude that the deviation is due to the thermodynamics of the system, i.e., to the presence of short range order.

Figure 2(b) gives an estimation of the equilibrium vacancy concentration c_v in these alloys as a function of c, as obtained from the mean-field expression of the vacancy formation energy E_v^f:

$$E_v^f(c) \approx cE_{v,Ni}^f + (1-c)E_{v,Cu}^f + Zc(1-c)\epsilon/2. \qquad (8)$$

As expected from Eq. (8), on a log-linear plot [see Fig. 2(b)], the vacancy concentration displays a linear dependence with c, with a small negative curvature for the $CuNi^{\epsilon}$ model, and no curvature for the $CuNi^0$ model. In the case of a coherent Cu/Ni multilayer, the equilibrium vacancy concentration in the Cu layers will exceed that of the Ni layers by about two and three orders of magnitude for $T=1000$ K and $T=650$ K, respectively.

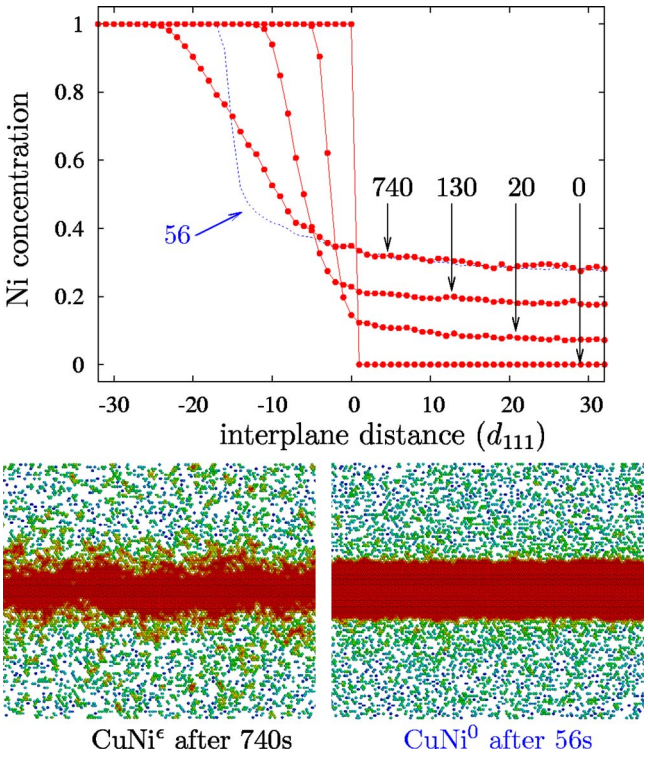

FIG. 3. (Color online) Instantaneous Ni concentration profiles and microstructures from initial sharp (111) interfaces in Cu/Ni multilayers for the $CuNi^{\epsilon}$ model alloy with $L_m=128$ planes and annealed at $T=650$ K. Note that $T_c\approx625$ K for that alloy. The KMC profiles (•) are obtained at different times $t=0$, 20, 130, and 740 s. For comparison (thin dotted line), one profile from KMC simulations of an ideal $CuNi^0$ multilayer ($T_c=0$ K) is reported at $t=56$ s. Below, the Ni atom positions in (111) plane intersecting the multilayer are shown in $CuNi^{\epsilon}$ at $t=740$ s and in $CuNi^0$ at $t=56$ s. The grey scale color is used to indicate the number of Ni neighbors of each Ni atom.

In summary, for a Cu/Ni multilayer, the diffusion coefficients calculated at constant c_v combined with the effect of the formation energy on c_v lead to a strong mobility asymmetry, $D^{Cu}_{Ni^*}/D^{Ni}_{Cu^*}\approx3\times10^2$ at $T=1000$ K and $\approx10^4$ at $T=650$ K. These ratios are almost the same for the two models, $CuNi^{\epsilon}$ and $CuNi^0$. The tendency for phase separation in the $CuNi^{\epsilon}$ model alloy, however, affects the composition dependence of the diffusion coefficients in concentrated alloys, particularly at low temperature, where short-range order becomes more and more significant.

III. INTERDIFFUSION IN Cu/Ni MULTILAYERS

A. Evolution of sharp and flat interfaces

In Fig. 3 we report the KMC Ni concentration profiles at different stages of the interdiffusion from the annealing of a Cu/Ni multilayer presenting initially sharp interfaces that are also flat, i.e., with no roughness, for the $CuNi^{\epsilon}$ model alloy. The simulation box contains 128^3 sites in the fcc structure with periodic boundary conditions. The annealing temperature is $T=650$ K. The initial concentration profile is a sym-

metric Ni/Cu multilayer of modulation length L_m equal to 128 (111) atomic planes with two (111) sharp interfaces and one vacancy V, corresponding to a vacancy concentration 4.77×10^{-7}.

As seen in Fig. 3, the interface broadens with time, but the center of the interface shifts to the Ni-rich region. Such an effect is indeed expected from the diffusion asymmetry present in this model alloy. Indeed, the vacancy is mainly found in the Cu-rich region and the Ni atoms that diffuse towards the Cu regions come essentially from Ni-vacancy exchanges at the interfaces. We note that, while this shift resembles the one that would be produced by a Kirkendall effect (markers at the initial interface position would now be in the Cu-rich region, i.e., in the region of the fast diffusers), its origin is fundamentally different since vacancies are treated as conserved species in the simulations, thus preventing the establishment of permanent vacancy flux. The interfacial shift in our simulations is a direct consequence of the composition dependence of the atomic diffusion coefficients. As the annealing proceeds, the Ni concentration of the initially pure Cu region increases, while the Cu concentration of the Ni-rich region remains null. As seen from Fig. 3, the kinetic paths for the $CuNi^0$ and $CuNi^\epsilon$ alloys are different. If one uses the average Ni concentration (c_{Ni}^{Cu}) inside the Cu region as a measure of the degree of advancement of the reaction, interfaces in the $CuNi^\epsilon$ display more broadening: after 740 s c_{Ni}^{Cu} has reached a value of about 0.28 and the Ni/Cu interfaces are largely spread over more than 20 (111) planes at $T=650$ K. On the other hand, in the $CuNi^0$ multilayer, for the same concentration $c_{Ni}^{Cu}\approx0.28$, the interface width is only 4 (111) planes.

In Fig. 3 we report the instantaneous Ni atom positions in one (111) plane that intersects the interfaces. From these snapshots, one can observe clear differences in interface morphology. Not only is the interface broader for the $CuNi^\epsilon$, it also appears to have developed some roughness. Since the $CuNi^\epsilon$ and the $CuNi^0$ multilayers differ only by the value of the phase-separation term ϵ, we conclude that the tendency toward phase separation tends to broaden and roughen interfaces in systems having large diffusion asymmetries.

To analyze in more details the effect of short-range order (SRO) on the interface broadening, we calculate for the $CuNi^\epsilon$ alloy the average interface width l_ϵ estimated as $l_\epsilon=d_{111}/\max(c_{p+1}-c_p)$ [where c_p is the instantaneous concentration in plane p and d_{111} is the (111) interplane distance] as a function of time in Fig. 4 and as a function of the Ni concentration at the center of the Cu region (c_{Ni}^{Cu}) in Fig. 5. Also reported in Figs. 4 and 5 is the interface width l_0 obtained from the KMC simulations of $CuNi^0$.

Figure 4 illustrates how interdiffusion is affected by short-range order. In absence of phase separation tendency (i.e., for l_0), one can observe from Fig. 4(a) a persistent layer-by-layer dissolution mode. Indeed, the main variation of concentration is found in the interface plane while the composition in other planes vary slowly. This leads to an oscillatory behavior of l_0 on top of the average increase of l_0 due to interfacial broadening. Note that for $T=650$ K and after 20 Ni layer dissolution in the Cu matrix, the amplitude of l_0 oscillations is still approximately conserved and the period of these oscillations roughly scales with $\sqrt{t}$. On the contrary, for $CuNi^\epsilon$ at the same temperature, one notices in Fig. 4(b) that the amplitude of the periodic oscillations of l_ϵ decreases rapidly. In this case, the concentration variation is not localized in the interface plane only, and dissolution occurs simultaneously in adjacent planes. This is consistent with the visual observation of the buildup of interfacial roughness. We conclude that short-range order, through the development of interfacial roughness, suppresses the layer-by-layer character of the interdiffusion reaction.

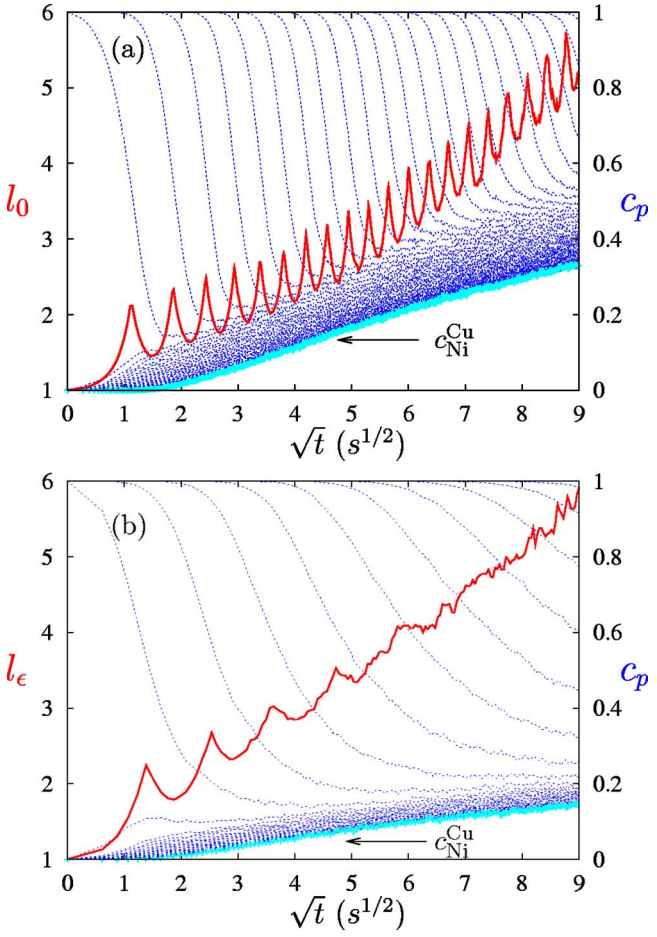

FIG. 4. (Color online) KMC interdiffusion in symmetrical (111) multilayer with initial sharp interfaces at $T=650$ K and $L_m=128$ planes (a) for $CuNi^0$ and (b) for $CuNi^\epsilon$. On the left axes, the interface width l [thick lines, in number of (111) interplane] is plotted versus the square root of time. On the right axes, the evolution of Ni concentrations c_p per plane p parallel to the initial flat interface (dotted lines) are reported. c_{Ni}^{Cu} (thick light grey) is the Ni concentration at the plane located at the center of the initial Cu region.

Let us now comment the curves shown in Fig. 5 (semilog plots) where two different annealing temperatures are considered, 650 and 1000 K). All curves start with $l=d_{111}$ and using this representation of the kinetics (l_ϵ versus the Ni concentration c_{Ni}^{Cu}), the interface widths start to increase before Ni atoms can reach the center of the Cu region (l_ϵ increases while c_{Ni}^{Cu} is still equal to zero). Furthermore, $\ln(l_\epsilon)$ and $\ln(l_0)$ obey a linear increase with the Ni concentration c_{Ni}^{Cu} with a slope $m(T)$ that depends on the temperature. The

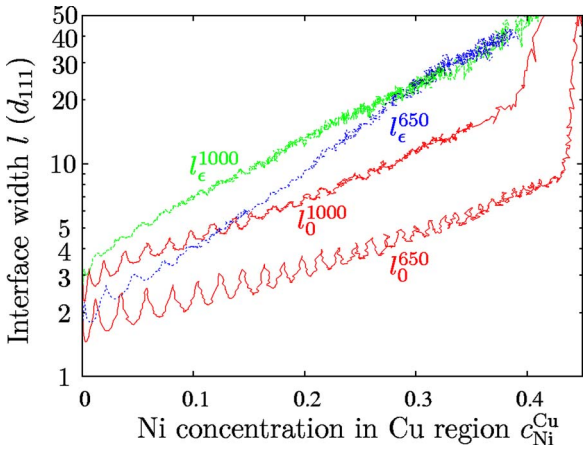

FIG. 5. (Color online) Interface width l versus the Ni concentration $c_{\mathrm{Ni}}^{\mathrm{Cu}}$ measured at the center of the initial Cu region. Calculations are obtained from KMC simulations performed at $T=650$ K and 1000 K with initial sharp (111) interfaces. l_ϵ and l_0 represent the interface widths for the CuNi^ϵ and CuNi^0 alloys, respectively.

temperature dependence of $m(T)$, however, exhibits opposite behaviors for l_ϵ and l_0. The slope $m(T)$ decreases when T decreases for l_0. This indicates that at lower temperatures, the interface broadening proceeds more slowly that the Ni enrichment of the Cu-rich region. On contrary, for l_ϵ, a decrease of the annealing temperature leads to an increase of the slope $m(T)$. The phase-separation tendency thus favors interfacial broadening over chemical mixing.

B. Evolution of diffuse and flat interfaces

To investigate the possible sharpening of Cu/Ni interfaces, following Erdélyi *et al.*,[3] we now construct a multilayer comprised of pure Cu and Ni regions separated by interfaces whose composition varies linearly, here over eight planes [see Fig. 6(a)]. Interdiffusion begins by the dissolution of the tail of the Ni-composition profile into the initially pure Cu region, while almost no Cu atom is found to diffuse into the initially pure Ni region. This asymmetric interdiffusion leads to a sharpening of the interface concentration profile as shown in Fig. 6(a). This sharpening is very similar to the one observed by Erdélyi *et al.* with a direct exchange mechanism. In a second stage, the Ni-pure regions start to dissolve into the Cu-rich regions, thus contributing further to the shift of the interface. This second stage produces a broadening of the interface. As a result, l_ϵ goes through a minimum, $\approx 3\, d_{111}$ for the simulation parameters used in Fig. 6(b).

We now examine the effect of SRO on the sharpening. For this purpose, we follow the minimum interface width (denoted $l_\epsilon^{\min}$ and $l_0^{\min}$) reached during the interdiffusion for various annealing temperatures. In Fig. 7(a), we report the temperature dependence of these minimum widths. We also report the equilibrium CuNi^ϵ interface widths l^{equil} (below the critical temperature $T_c=625$ K) and the minimum interface width $l_{\mathrm{sym}}^{\min}$ obtained in absence of diffusion asymmetry. For that purpose we used a new set of parameters such that $\epsilon=-0.022$ eV, with $E_0^{\mathrm{A}}=E_0^{\mathrm{B}}$, $E_2^{\mathrm{A}}=E_2^{\mathrm{B}}$, and $u=0$ giving a zero

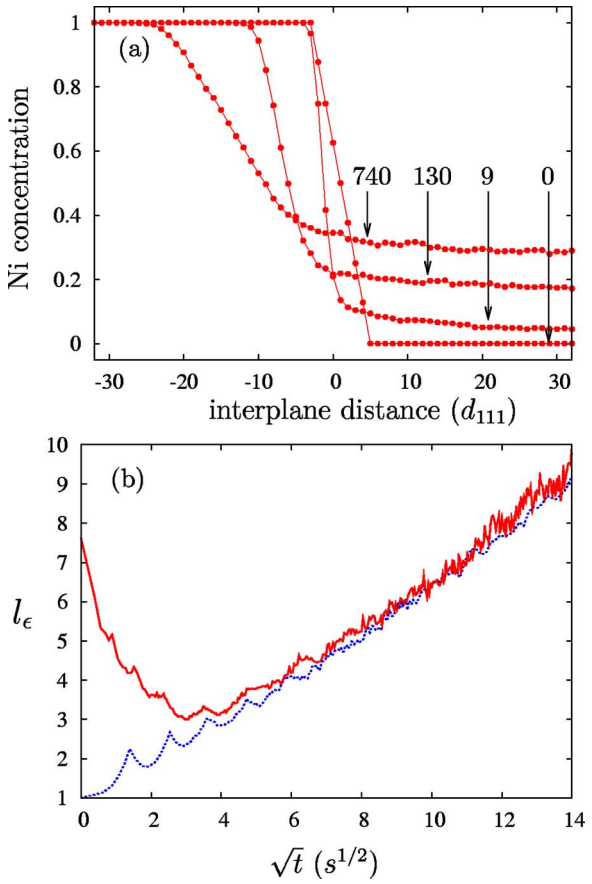

FIG. 6. (Color online) KMC simulations from symmetrical (111) multilayer ($L_m=128$ planes) with initial diffuse interfaces $[l_\epsilon(t=0)\approx 8d_{111}]$ for the CuNi^ϵ model alloy at $T=650$ K: (a) instantaneous Ni concentration profiles (b) interface width l_ϵ [solid line, in number of (111) planes] versus the square root of time. For comparison the l_ϵ evolution obtained from sharp interface is replotted (dotted line).

value of the diffusion asymmetry term $\ln(D_{B^*}^A/D_{A^*}^B)$. For this system, although there is no asymmetry in diffusion coefficient, the interface width also reaches a minimum transient value $l_{\mathrm{sym}}^{\min}$ before relaxing towards l^{equil}, because of the nonzero value of ϵ.

Figure 7(a) shows that $l_0^{\min}$ and $l_\epsilon^{\min}$ decrease similarly with temperature. One can notice, however, that $l_0^{\min}$ is about one plane lower than $l_\epsilon^{\min}$. Again, this illustrates the influence of short-range order. The later produces some interfacial roughness, which then reduces the sharpening effect. We now compare the transient minimum widths with the equilibrium ones. Indeed, Erdelyi *et al.*[4] indicated recently that if the diffusion asymmetry is large enough, the interface could be even sharper than its equilibrium value, for a relatively strong phase-separation system. This is indeed what we observe for our present model alloys, as seen from Fig. 7(a). Below ≈ 550 K, however, $l_\epsilon^{\min}$ appears to increase with decreasing temperatures, which is possibly due to a larger and larger driving force for phase separation. This latter result shows that the coupling between the phase separation and large diffusion asymmetry is not straightforward. Indeed, since both driving forces tend to sharpen the initial interface

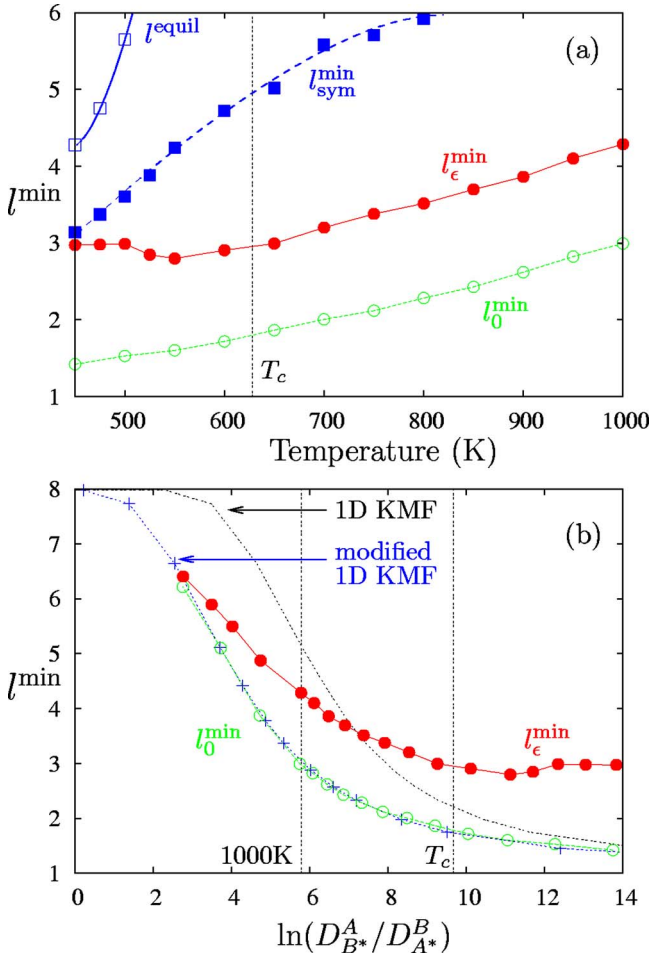

FIG. 7. (Color online) Minimum interface widths (•) l^{min}_{ϵ} for CuNi$^{\epsilon}$ and (◦) l^{min}_{0} for CuNi^{0} alloy [in the number of (111) planes] reached during the KMC sharpening of initial diffuse interfaces [$l_{\epsilon}(t=0)=l_0(t=0)\approx 8d_{111}$] versus (a) the annealing temperature and (b) the diffusion asymmetry $\ln(D^A_{B^*}/D^B_{A^*})$. In (a) the equilibrium interface width (□) l^{equil} is calculated for the CuNi$^{\epsilon}$ model alloy and (■) l^{min}_{sym} corresponds to the minimum transient width obtained for an alloy having the same phase-separation tendency but no diffusion asymmetry (see text). In (b) the l^{min}_{0} obtained from the one-dimensional kinetic mean-field model (1D KMF) is reported (dotted curve) before and (+) after the modification of this model discussed in the text.

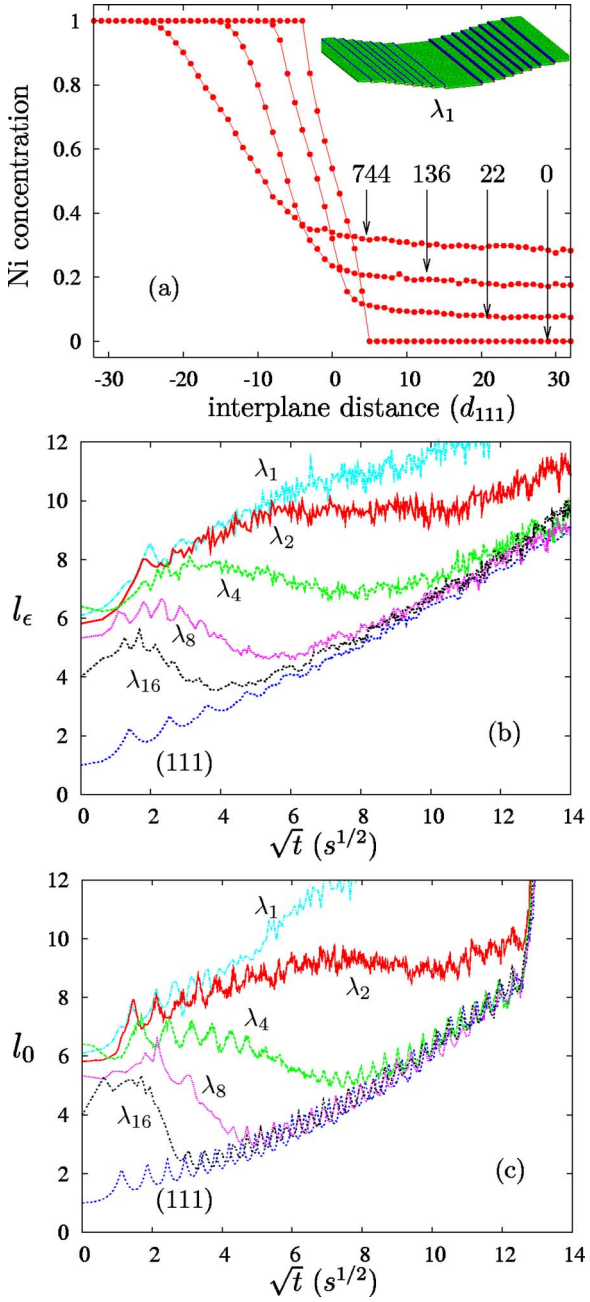

FIG. 8. (Color online) (a) KMC Ni concentration profiles for CuNi$^{\epsilon}$ at $T=650$ K, at different stages of the kinetics. The initial interface is a sinusoid of wavelength $\lambda_1=64\sqrt{3/2}a$ and of amplitude $A=4d_{111}$. In (b) for CuNi$^{\epsilon}$ and in (c) for CuNi^{0}, interface widths [in number of (111) planes] are given as a function of the square root of time $\sqrt{t}$, for different initial wavelengths $\lambda_n=\lambda_1/n$ but for the same amplitude $A=4d_{111}$. The curves obtained from sharp (111) interfaces are also reported for comparison.

[both l^{min}_{sym} and l^{min}_{0} are lower than eight planes in Fig. 7(a)], one could have expected l^{min}_{ϵ} values lower than l^{min}_{0}. The observation that $l^{min}_{sym}>l^{min}_{\epsilon}>l^{min}_{0}$ shows that these sharpening effects are not simply additive. At low temperature the l^{min}_{ϵ} curve becomes close to the l^{min}_{sym} one [see Fig. 7(a)], while at high temperature l^{min}_{ϵ} and l^{min}_{0} display similar behaviors [see Fig. 7(b)].

In Fig. 7(b), we replot the data from Fig. 7(a) for l^{min}_{ϵ} and l^{min}_{0} but now using the mobility asymmetry $\ln(D^A_{B^*}/D^B_{A^*})$ for the abscissa. The two vertical lines indicate the mobility asymmetry for $T=1000$ K and for $T=T_c$. In absence of phase separation, i.e., $\epsilon=0$ in the activation energies, we recover qualitatively the trend obtained from the 1D mean-field model (1D KMF) used by Erdélyi *et al.*[3] the sharpening increases with the mobility asymmetry [l^{min}_{0} decreases with $\ln(D^A_{B^*}/D^B_{A^*})$]. However, we notice that the 1D KMF model used in Ref. 3 with one effective asymmetry parameter is not suitable for predicting quantitatively the dependence of l^{min}_{0} with $\ln(D^A_{B^*}/D^B_{A^*})$. Figure 7(b) suggests in fact a modification of the 1D KMF model to obtain a quantitative agreement with our 3D KMC data. The idea is to introduce a second effective parameter (denoted K here) that will shift the 1D

KMF curve to the left. Recall that in the 1D KMF model $\ln(D^A_{B^*}/D^B_{A^*})=Zu/kT$. From a purely phenomenological viewpoint, one could replace Zu/kT by $Zu/kT+K$. As seen in Fig. 7(b), an excellent agreement is obtained for $K=-2.1$. As discussed in the Appendix, this second effective asymmetry parameter is equivalent to introducing a dependence of the attempt frequencies with the local environment, which can also been seen as the effect of the mobility asymmetry on correlation factors. Despite the fact that this approach is purely phenomenological, it is interesting to see that a modified kinetic mean-field model based on a direct atom exchange mechanism, with two effective asymmetry parameters, can reproduce quantitatively (at least when $\epsilon=0$) the interface sharpening process observed with a more sophisticated approach, i.e., 3D kinetic Monte Carlo simulations with a vacancy mechanism.

C. Evolution of sharp but rough interfaces

In this section, we follow the evolution of interfaces that are sharp but rough. For ease of analysis, we use one-dimensional sinusoidal sharp interfaces, with a wave vector along a $\langle 110\rangle$ direction perpendicular to the [111] direction of the interface. The initial interface height at position $\mathbf{r}=(r_x,r_y)\in(111)$ and at time $t=0$ is given, in units of d_{111}, as

$$h(\mathbf{r},0)=\langle h(\mathbf{r},0)\rangle+A\sin\left(\frac{2\pi}{\lambda_n}r_x\right), \tag{9}$$

where the x axis is along the in-plane $[11\bar{2}]$ direction, $\langle h(\mathbf{r},0)\rangle$ is the initial average height of the interface considered (the brackets denote an average over all possible $\mathbf{r}$), and A and λ_n are the initial amplitude and wavelength of the sinusoid, respectively. An example of such an interface is shown in the inset of Fig. 8(a) where Ni atoms from one interface are drawn for $A=4d_{111}$ and $\lambda_n=\lambda_1=64\sqrt{3/2}a$. Note that the terraces end with $[1\bar{1}0]$ steps. The composition profiles of these interfaces, obtained by averaging the composition in successive (111) planes, display an apparent diffuseness, as seen in Fig. 8(a) for time $t=0$. No apparent sharpening is observed for this interface during annealing at $T=650$ K. The apparent width of the interface increases monotonously with time, and the interface position shifts to the Ni-rich region.

To provide a quantitative analysis of this phenomenon, we report in Figs. 8(b) and 8(c) the time dependence of the interface widths l_ϵ and l_0 for different initial wavelengths $\lambda_n=\lambda_1/n$ values. These figures demonstrate the strong role played by the initial wavelength. For large wavelengths (e.g., λ_1), l_ϵ and $l_0\approx 6d_{111}$ initially, and these widths increase continuously with time, in a manner similar to the one observed for a sharp (111) interface in Sec. III A. For small wavelengths, on the other hand, one observes an interface sharpening analogous to the one seen for interfaces that are initially diffuse but flat in Sec. III B. The threshold wavelength λ_c above which there is no interface sharpening can be bracketed. At $T=650$ K, for $A=4d_{111}$, we obtained $\lambda_8<\lambda_c<\lambda_4$ and $\lambda_4<\lambda_c<\lambda_2$ for $CuNi^\epsilon$ and $CuNi^0$, respectively. Additional simulations with different system sizes could be used to further refine the determination of λ_c, if necessary.

From Figs. 8(b) and 8(c), it is also interesting to note that below λ_c, the sharpening is followed by an interface broadening analogous to the one observed for an initial (111) sharp interface. In other words, for symmetrical A/B multilayers that have the same average interface orientation and the same quantity of A and B atoms per (111) layers, the interface broadening at long time becomes independent of the initial interface roughness. This point suggests that two distinct mechanisms take place simultaneously: the first mechanism, which depends on the wavelength, tends to flatten the initial sinusoidal profile, while the second mechanism induces a broadening of the interfaces. In order to test this assumption, we need to separate and quantify the roughness and the diffuseness of the interfaces. For this purpose, we calculate the height-to-height correlation function $G(\mathbf{R},t)$:

$$G(\mathbf{R},t)=\langle[h(\mathbf{r}+\mathbf{R},t)-h(\mathbf{r},t)]^2\rangle^{1/2}, \tag{10}$$

where the vector $\mathbf{R}=(R_x,R_y)\in(111)$ corresponds to the in-plane component of the vector separating the interfacial atoms located at $\mathbf{r}+\mathbf{R}$ and at $\mathbf{r}$. Before calculating $G(\mathbf{R},t)$ we first perform a coarse graining of the initial fcc lattice into a simple cubic lattice; the coarse-grained lattice (CGL) contains one-fourth of the fcc sites and each CGL site belongs to the Ni-rich phase if the number of Ni first and second neighbors in the fcc lattice is greater than 9 (corresponding to a Ni local concentration greater than 0.5). The Ni-rich phase is identified as the largest connected set of such sites. Interfacial CGL sites in the Ni-rich phase are those which have at least one CGL first neighbor in the opposite phase. Finally since the sinusoidal perturbation considered in Eq. (9) is along the x axis, the $G(\mathbf{R},t)$ function is averaged over all $\mathbf{R}$ having the same R_x component. In Fig. 9, starting from sinusoidal interfaces with $\lambda_n=\lambda_4$ for the $CuNi^0$ system, we plot a sequence of instantaneous configurations and the corresponding $G^2(\mathbf{R},t)$ (semilog plots). In Fig. 9(a), the initial $G^2(\mathbf{R},0)$ is given by a cosine function, with a period of λ_4. In Figs. 9(b) and 9(c), during the sharpening regime [i.e., during the l_0 decrease in Fig. 8(c)], one can observe both the shift and the flattening of the interfaces. A signature of this latter phenomenon in the $G^2(\mathbf{R},t)$ plots is the decrease of the amplitude of the cosine. Two additional observations can made from the $G^2(\mathbf{R},t)$ plots: first, the initial wavelength is conserved during the interface flattening, and second the average value of the $G^2(\mathbf{R},t)$ function increases with time. Finally in Fig. 9(d), which corresponds in Fig. 9(c) to the time where l_0 starts to increase, interfaces appear to be flat and diffuse, and the $G^2(\mathbf{R},t)$ is nearly constant. It is observed that, at longer times, this constant value increases with time (not shown here).

We now propose a simple model to analyze quantitatively these kinetic evolutions. We assume that the time evolution of the interface shape can be decomposed into two terms:

$$h(x,t)=\frac{A(t)}{2}\left[1+\sin\left(\frac{2\pi}{\lambda_n}x\right)\right]+B(t)\,\eta(x), \tag{11}$$

where $A(t)$ gives the amplitude of the sinusoid. It decreases with time and corresponds to flattening of the interface. Note

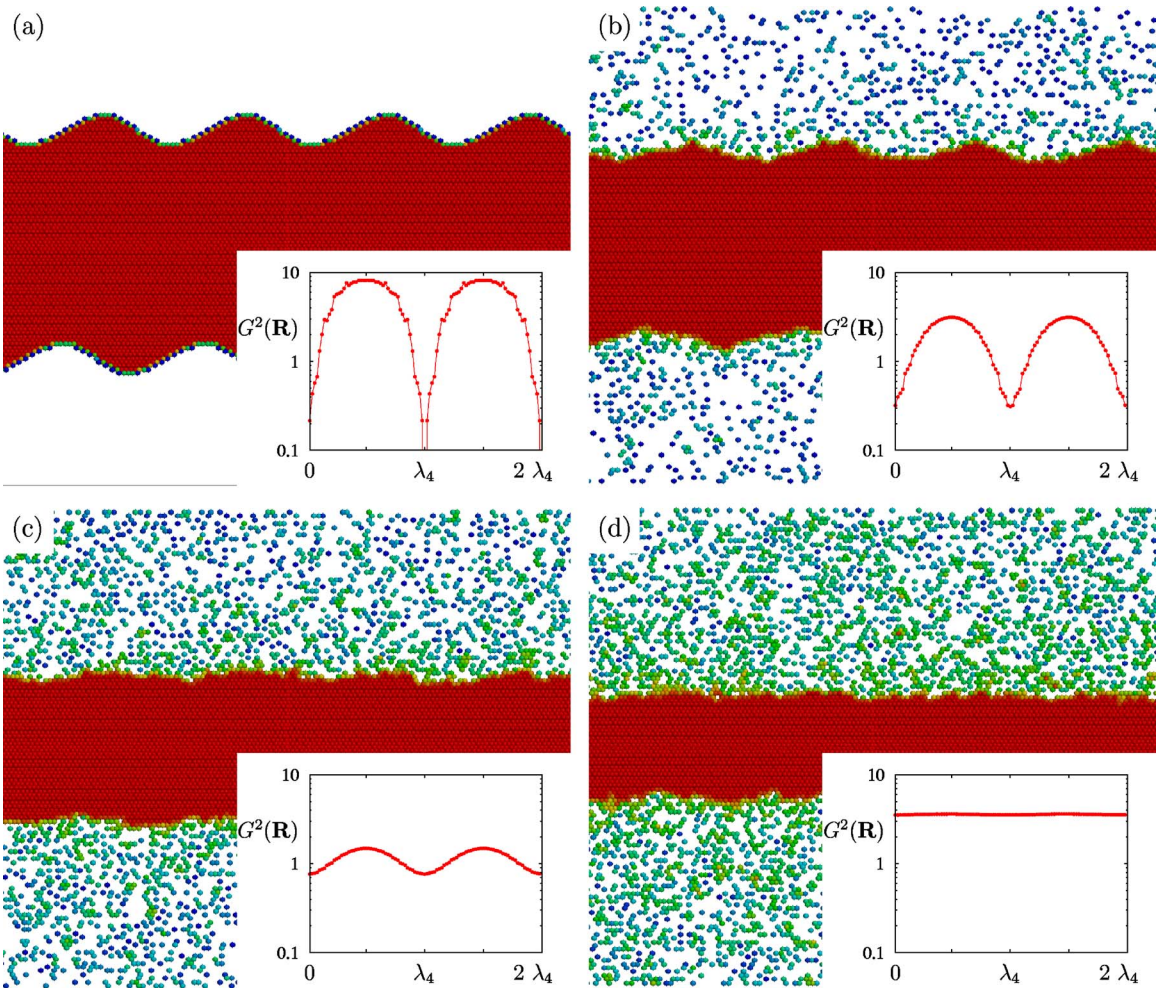

FIG. 9. (Color online) Sequence of microstructures [Ni atoms from one (111) plane only] and height difference correlation function $G^2(\mathbf{R},t)$ at different stage of the kinetics: $\sqrt{t_i}=0$ in (a), 4 in (b), 6 in (c), and 8 in (d) from a $CuNi^0$ multilayer with wavelength λ_4 amplitude $A=4d_{111}$ and $T=650$ K.

that the previous observations indicate that $A(t)$ is likely to be a function of λ_n. $B(t)$, on the other hand, represents the amplitude of the diffuseness, and it is expected to increase with time and to be independent of λ_n. $\eta(x)$ is an uncorrelated random variable that has a configurational average $\langle\eta(x)\rangle=1/2$ with $\eta(x)\in[0:1]$. The average interface height is $\langle h(x,t)\rangle=[A(t)+B(t)]/2$ and the square of the interface width defined as

$$\sigma(t)^2=\langle h(x,t)^2\rangle-\langle h(x,t)\rangle^2=\frac{A(t)^2}{8}+\frac{B(t)^2}{12}, \qquad (12)$$

since we assume that the two contributions in the right-hand side of Eq. (11) are uncorrelated. Finally, using the definition of Eq. (10), the square of the height-to-height correlation function $G(X,t)^2=\langle[h(x+X,t)-h(x,t)]^2\rangle$ writes

$$G(X,t)^2=\frac{A(t)^2}{4}\left[1-\cos\left(\frac{2\pi}{\lambda_n}X\right)\right]+\frac{B(t)^2}{6}. \qquad (13)$$

From Eq. (13), it is interesting to note that one can extract both $A(t)$ and $B(t)$ amplitudes by evaluating the $G(X,t)^2$ function for two different values of X. Indeed, for $X=\lambda_n$, one obtains the diffuseness of the interface $B(t)^2=6G(\lambda_n,t)^2$, and then, by evaluating the correlation function at $X=\lambda_n/2$, one deduces the sinusoid amplitude $A(t)^2=2[G(\lambda_n/2,t)^2-G(\lambda_n,t)^2]$.

A first consistency test for the present analysis, and in particular for the assumption that the two contributions in Eq. (11) are uncorrelated, is performed by comparing the time evolution of the $G(\lambda_n,t)^2$ functions for various initial wavelengths and amplitudes. Since we model interfaces that are initially sharp, we expect that $B(0)=0$ in all cases, and that the time evolution of $B(t)$ should be the same for all $A(0)$ and λ_n. This is indeed what is observed in Fig. 10 for $A(0)=4d_{111}$. This evolution, furthermore, is very similar to the one found for the initially sharp and flat interface considered in Sec. III A. For $A(0)=16d_{111}$, we observe some dependence of the evolution of $B(t)$ with the wavelength. These deviations, however, remain small in comparison to the large $A(t)$ values.

We now use Eqs. (11) and (13) to study the decrease of amplitude $A(t)$ as a function of time, initial amplitude, and initial wavelength. In Figs. 11(a) and 11(b), we report calculations of the $G(\lambda_n/2,t)^2-G(\lambda_n,t)^2$ function, which is pro-

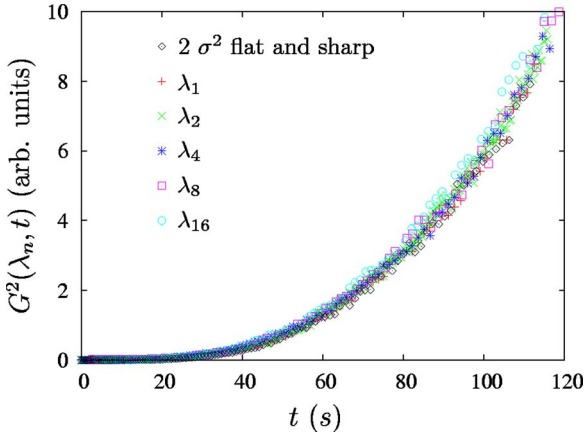

FIG. 10. (Color online) Height difference correlation functions $G^2(\lambda_n,t)$ versus time from sinusoidal interfaces having different initial wavelengths λ_n, same initial amplitude $A=4d_{111}$, at $T=650$ K, for the $CuNi^0$ model alloy. The $G^2(\lambda_n,t)$ functions are compared to the square of the interface width $\sigma^2(\times 2)$ calculated from the KMC simulations of $CuNi^0$ multilayers with initial flat and sharp interfaces.

portional to $A(t)^2$, for the $CuNi^0$ and $CuNi^\epsilon$ systems, respectively. Clearly, the decrease of $A(t)$ with time is well described by an exponential decay. Moreover, we find that the corresponding relaxation times τ increase with the value of the initial wavelength, in agreement with the observation made from Fig. 8.

It is useful to recall that, in the case of systems possessing interfaces at equilibrium, Mullins[24] predicted that perturbations of the interface position would relax exponentially in time. Furthermore, the relaxation time constant is predicted to depend on the wavelength through a power law, $\tau \propto \lambda_n^\alpha$, where the exponent α takes a value characteristic of the relaxation mechanism. Viscous relaxation leads to $\alpha=1$, evaporation condensation to $\alpha=2$, bulk diffusion to $\alpha=3$, and surface diffusion to $\alpha=4$. Even though we are monitoring here the amplitude of perturbations of interfaces that are not stable, the relaxation of $A(t)$ appears to be fast compared to the dissolution kinetics, and this relaxation kinetics may thus contain some useful information on the mechanisms involved. For the $CuNi^\epsilon$ system, an average apparent exponent of $\alpha \approx 1.8$ is obtained. This is not too different from 2, the exponent expected for stable interfaces whose relaxation is controlled by evaporation-condensation. We also note that at $T=650$ K, the system is only slightly above its critical temperature, which increases the transient stability of A/B interfaces. The parallel between the two exponents, 1.8 and 2, appears to be physically relevant since, for the alloys and parameters used here, we expect the relaxation to proceed by the detachment of Ni atoms from interfacial steps and step edges, followed by their fast diffusion into the Cu-rich regions of the multilayer. Further work is required to determine whether the relaxation time τ is independent the initial amplitude, as expected in the case of relaxation of equilibrium interfaces. For $CuNi^0$ system, the time constant τ appears to be independent of the initial amplitude, with a value $\alpha \approx 1.2$, or $\alpha \approx 1.1$ if one excludes the data for λ_1. It was expected that a different exponent could be observed for this

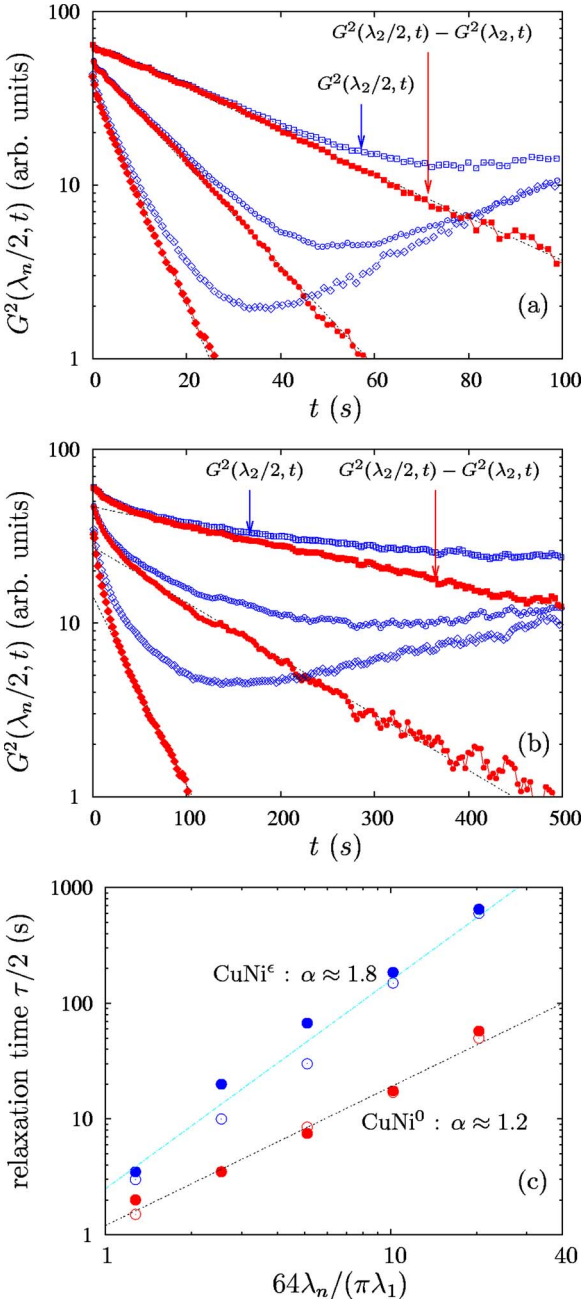

FIG. 11. (Color online) Height difference correlation functions $G^2(\lambda_n,t)$ and $G^2(\lambda_n/2,t)-G^2(\lambda_n,t)$ versus time (semilog plots) from different sinusoidal interfaces: $n=2$(□, ■), $n=4$(○, •), and $n=8$(◇, ◆) at $T=650$ K and from the same initial amplitude $A=16d_{111}$ for (a) $CuNi^0$ and (b) $CuNi^\epsilon$ multilayers. In (c) the relaxation times τ (s) are plotted as a function of the initial wavelength from two initial amplitudes $A=4d_{111}$(○) and $A=16d_{111}$(•).

system, since the probability for Ni atoms detachment from interfacial sites is not controlled at all by internal energy gain or loss, but solely by configurational entropy and kinetics. In fact, as the wavelength of the perturbation decreases, for a fixed amplitude $A(0)$, the number of interfacial steps increases linearly with λ_n. More works is needed to establish whether this simple explanation is indeed at the origin of the apparent exponent close to 1 for the $CuNi^0$ system.

Based on the above results, we now introduce a simple kinetic model to analyze the competition between the exponential smoothening identified in the previous paragraph and the broadening due the intermixing of the Cu and Ni atoms. These two contributions correspond to the kinetic evolution of the terms $A(t)^2/8$ and $B(t)^2/12$ in Eq. (12). In the case of a broadening due to the random migration of atoms, $B(t)^2$ should increase linearly with time. The results obtained in Sec. III A, where we consider interfaces that were initially perfectly sharp and flat, i.e., $A(0)=B(0)=0$, are broadly consistent with this behavior. Indeed, for the CuNi$^{\epsilon}$ system, the interface width l_{ϵ} increases roughly linearly with the square root of time. For the CuNi^0 system, the agreement is less satisfactory, but the main trend is preserved. We can thus propose that, for initially sharp but rough interfaces, the kinetic evolution of the total interface width $\sigma(t)^2$ follows:

$$\sigma(t)^2 = C_0 A(0)^2 \exp\left(-\frac{t}{\tau}\right) + C_1\left(\frac{t}{\tau_1}\right), \tag{14}$$

where the relaxation time $\tau = C\lambda_n^{\alpha}$, whereas the relaxation time τ_1 is a constant independent of λ_n and C, C_1, C_2 are constants. Simple algebra shows that, for $\sigma(t)^2$ to reach a minimum, the following inequality has to be satisfied:

$$\frac{C_0}{C_1}\frac{\tau_1}{\tau}A(0)^2 > 1. \tag{15}$$

There is therefore a maximum wavelength of the initial roughness λ_c, above which no sharpening will take place:

$$\lambda_c = \left[\frac{C_0}{C_1}\frac{\tau_1}{C}A(0)^2\right]^{1/\alpha}. \tag{16}$$

This simple model thus indicates that the existence of a maximum wavelength for the apparent sharpening of interfaces results from the competition between a wavelength-dependent smoothening and wavelength-independent broadening. Similarly, Eq. (15) predicts that, for a given wavelength, there is a minimum initial roughness amplitude for the apparent sharpening to take place. The results obtained in Sec. III A, where $A^2(0)=0$, and Sec. III C, where $A^2(0)>0$, are certainly compatible with this conclusion.

IV. CONCLUSIONS

In this paper we investigate the kinetics of interdiffusion in Cu/Ni multilayers by using kinetic Monte Carlo simulations with a diffusion model based on a atom-vacancy exchange mechanism. Activation energies for the vacancy-atom exchanges are adjusted in order to reproduce quantitatively the five jump frequencies that control the self- and solute diffusion coefficients for Ni and Cu tracer atoms. In this fitting procedure, the activation barriers calculated by Adams *et al.*[19] with an EAM interatomic potential serve as a reference. This parametrization produces a strong mobility asymmetry, $D^{\mathrm{Cu}}_{\mathrm{Ni}^*} \gg D^{\mathrm{Ni}}_{\mathrm{Cu}^*}$, as expected from the large differences in vacancy migration and vacancy formation energies, ΔE^m and ΔE^f. Additionally, to investigate the influence of short-range order on the interdiffusion, we have used two sets of parameters, which have the same kinetics parameters but differ by the value of the ordering energy parameter ϵ. In one set, CuNi^0, $\epsilon=0$ and it corresponds therefore to an alloy system forming an ideal solid solution, whereas in the second set, CuNi$^{\epsilon}$, ϵ is set to a negative value that results in an system with a small phase-separation tendency, with a critical temperature $T_c \approx 625$ K, close to the experimental one. The main results obtained in this work are the following:

(i) By performing KMC simulations on equilibrium Cu-Ni solid solutions, we measure the composition dependence of tracer diffusion coefficients. We show that marked deviations from a simple exponential dependence with composition appear at low temperature in the CuNi$^{\epsilon}$ system.

(ii) We study the kinetics of interdiffusion after the annealing, above T_c, of (111) Cu/Ni symmetrical multilayers with interfaces that are initially sharp and flat. We observe an interface shift, with Ni atoms filling up the Cu region, as expected from the works by Erdélyi and co-workers works.[2–4] Then we study the role of the phase-separation tendency (ϵ) on the interface broadening. For the same amount of Ni atoms having diffused in the Cu region, the interface width can be much larger in presence of short-range order. For the same diffusion asymmetry, interfaces broaden more in an alloy system that displays phase separation at low temperature.

(iii) In Sec. III B, we study diffuse but flat (111) interfaces, and we observe a transient interface sharpening in our model Cu-Ni systems, for annealing temperatures of 650 and 1000 K. These results confirm that the sharpening effect, which was first observed using an atom-atom exchange mechanism, can still be obtained with an atom-vacancy exchange model, as infered by Erdélyi *et al.*[3] We measure the minimum width reached by the interfaces and we show that the phase-separation tendency reduces the amplitude of the interface sharpening effect, due to the formation of interfacial roughness. We also compare the interface width obtained from our vacancy model with that predicted by the one-dimensional effective atom exchange model of Erdélyi *et al.*[3] We show that, in the case of an ideal solid solution, a simple, phenomenological extension of the kinetic mean-field model is sufficient to reproduce quantitatively the minimum widths obtained here with KMC simulations.

(iv) In Sec. III C we study the evolution of interfaces that are sharp but sinusoidally rough. If analyzed by a one-dimensional profile, this sinusoidal roughness contributes to the apparent diffuseness of the interfaces, in addition to their true diffuseness. We demonstrate that this apparent diffuseness, in contrast to the true diffuseness of the interface, may not display any transient sharpening. Indeed, we identify the existence of a threshold wavelength for the initial roughness, above which the apparent diffuseness of the interfaces will never decrease during annealing. This threshold wavelength is observed to increase when short-range order is present, i.e., for the CuNi$^{\epsilon}$ system. In order to quantify and analyze the kinetics of the interfacial evolution, we calculate the height-to-height correlation function of the interfaces. We demonstrate that the evaluation of this correlation function for different separation distances makes it possible to separate the diffuseness of the interface from its roughness. The amplitude of the roughness decreases exponentially with

time, with a relaxation time that displays a power-law dependence with the wavelength of the roughness. For small wavelength the relaxation time becomes smaller and smaller. The characteristic time for the buildup of the diffuseness of the interface, on the other hand, is independent of the initial wavelength of a sharp and sinusoidal profile. This simple analysis suggests therefore that there is a crossover wavelength λ_c, in agreement with the KMC results: for roughness with wavelength less than λ_c, an apparent sharpening of the interface can take place, whereas for roughness with wavelength greater than λ_c no transient sharpening will take place. Besides the interest in understanding the competition between interfacial smoothening and interfacial broadening, this result points to a limitation to the annealing method proposed by Erdélyi *et al.*[5] to sharpen interfaces in miscible alloy systems. We hope that the present results will stimulate experimental studies aimed at investigating the influence of the wavelength and the amplitude of the initial roughness on the phenomenon of transient interfacial sharpening.

ACKNOWLEDGMENTS

Helpful discussions with M. C. Benoudia, S. Labat, O. Thomas, Z. Erdélyi, I. A. Szabó, and D. L. Beke are gratefully acknowledged.

APPENDIX: EXTENSION OF THE 1D MEAN-FIELD MODEL

In practice and using for instance the formalism of Ref. 4, the slight modification suggested in this work means that the usual mean-field jump frequency $\Gamma_{i,i+1}$ for an effective exchange between an A atom in plane i and a B one in plane $i+1$ can be rewritten as follows:

$$\Gamma_{i,i+1} = \nu_{i,i+1}\exp\left(\frac{E_{i,i+1}}{kT}\right), \tag{A1}$$

where the effective attempt frequency $\nu_{i,i+1}$ now depends on the chemical environment and on the new parameter K:

$$\nu_{i,i+1} = \exp[z_v(c_{i-1} + c_i + c_{i+1} + c_{i+2}) + z_l(c_i + c_{i+1})]K/2Z. \tag{A2}$$

[1] E. Kirkendall, L. Thomassen, and C. Upthegrove, Trans. AIME **133**, 186 (1939).
[2] Z. Erdélyi, D. L. Beke, P. Nemes, and G. A. Langer, Philos. Mag. A **79**, 1757 (1999).
[3] Z. Erdélyi, I. A. Szabó, and D. L. Beke, Phys. Rev. Lett. **89**, 165901 (2002).
[4] Z. Erdélyi, G. L. Katona, and D. L. Beke, Phys. Rev. B **69**, 113407 (2004).
[5] Z. Erdélyi, M. Sladecek, L. M. Stadler, I. Zizak, G. A. Langer, M. Kis-Varga, D. L. Beke, and B. Sepiol, Science **306**, 1913 (2004).
[6] G. Martin, Phys. Rev. B **41**, 2279 (1990).
[7] M. Athènes, P. Bellon, G. Martin, and F. Haider, Acta Mater. **44**, 4739 (1996).
[8] J. M. Roussel and P. Bellon, Phys. Rev. B **63**, 184114 (2001).
[9] Lorenz -M. Stadler, B. Sepiol, R. Weinkamer, M. Hartmann, P. Fratzl, J. W. Kantelhardt, F. Zontone, G. Grubel, and G. Vogl, Phys. Rev. B **68**, 180101(R) (2003).
[10] P. Ehrhart, *Landolt-Börnstein: Numerical Data and Functional Relationships in Science and Technology*, New Series, Vol. III, Part 25 (Springer, Heidelberg, 1991).
[11] *Binary Alloy Phase Diagrams*, 2nd. ed., edited by T. B. Massalski, H. Okamoto, P. R. Subramanian, and L. Kacprzak (ASM International, Materials Park, OH, 1990).
[12] V. M. López-Hirata, T. Sakurai, and K. I. Hirano, Scr. Metall. Mater. **26**, 99 (1992).
[13] V. M. López-Hirata and K. I. Hirano, J. Mater. Sci. **31**, 1703 (1996).
[14] V. Holý and T. Baumbach, Phys. Rev. B **49**, 10668 (1994).
[15] T. Salditt, T. H. Metzger, and J. Peisl, Phys. Rev. Lett. **73**, 2228 (1994).
[16] A. T. G. Pym, A. S. H. Rozatian, C. H. Marrows, S. D. Brown, L. Bouchenoire, T. P. A. Hase, and B. K. Tanner, J. Phys. D **38**, A190 (2005).
[17] C. Schug, H. Grimm, R. Berger, A. Dietzel, and M. Wormington, Surf. Interface Anal. **36**, 908 (2004).
[18] A. Bieber, F. Gautier, G. Tréglia, and F. Ducastelle, Solid State Commun. **39**, 149 (1981).
[19] J. B. Adams, S. M. Foiles, and W. G. Wolfer, J. Mater. Res. **4**, 102 (1989).
[20] J. R. Manning, in *Diffusion Kinetics for Atoms in Crystals* (D. Van Nostrand Company, Inc., Princeton, 1968).
[21] A. R. Allnatt and A. Lidiard, in *Atomic Transport in Solids* (Cambridge University Press, Cambridge, England, 1993).
[22] F. Soisson, A. Barbu, and G. Martin, Acta Mater. **44**, 3789 (1996).
[23] M. Athènes, P. Bellon, and G. Martin, Philos. Mag. A **76**, 565 (1997).
[24] W. W. Mullins, J. Appl. Phys. **30**, 77 (1959).